NASA TN D-96

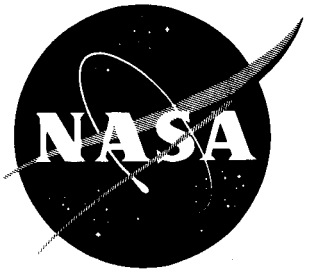

TECHNICAL NOTE
D-96

A METHOD FOR CALCULATING AERODYNAMIC LOADINGS ON THIN WINGS AT A MACH NUMBER OF 1

By John L. Crigler

Langley Research Center
Langley Field, Va.

NATIONAL AERONAUTICS AND SPACE ADMINISTRATION

WASHINGTON November 1959

NATIONAL AERONAUTICS AND SPACE ADMINISTRATION

TECHNICAL NOTE D-96

A METHOD FOR CALCULATING AERODYNAMIC LOADINGS ON THIN WINGS AT A MACH NUMBER OF 1

By John L. Crigler

SUMMARY

A method for calculating the aerodynamic loadings on thin wings at a Mach number of 1.0 is presented. The method differs from previously developed lifting-surface procedures in that the chordwise integrations are performed analytically and thus the need for numerical procedures is eliminated. The spanwise integrations are then performed by numerical procedures. A detailed description of the method is included.

Calculated results are compared with experimental data for a swept-wing—body configuration. The wing $\frac{1}{4}$-chord line was swept back 45°; the wing had an aspect ratio of 4 and a taper ratio of 0.15. The wing airfoil section at the midspan was NACA 64A206, a = 0 which faired into an NACA 64A203, a = 0.8 (modified) airfoil section at the 0.5-semispan location and retained this section from the midspan to the wing tip.

The magnitude and the distribution of the spanwise loading of the calculated data at a free-stream Mach number M_o of 1.0 are in good agreement with experimental data obtained at M_o = 0.98 and 1.03. No experimental data were obtained at M_o = 1.0.

INTRODUCTION

The linearized theory of compressible flow for the calculation of the aerodynamic loadings on thin wings of low aspect ratio at sonic speeds has been used by a number of authors (e.g., refs. 1 to 3). Also some discussion of the justification of the use of linearized theory for this purpose within the framework of the nonlinear theory for transonic flow is given in reference 4. Others (e.g., refs. 5 and 6) have devised numerical procedures for treating finite-aspect-ratio wings for incompressible flow. These procedures are easily adaptable to compressible flow and in reference 7 a method for calculating the aerodynamic loading on a wing in the speed ranges approaching a free-stream Mach number M_o of 1.0 is outlined. The method of reference 7 is similar to that developed by Falkner in reference 5 for treating wings in incompressible flow.

Calculated results of the magnitude of the load and the distribution of the spanwise loading shown in reference 7 were generally in good agreement with experimental data for all Mach numbers up to $M_o = 0.98$. Calculations were also made in reference 7 for the case of $M_o = 1.0$ (the procedure is not applicable at Mach numbers greater than 1) but the agreement in this case was somewhat poorer than it was for subsonic Mach numbers. Reference 8 presents a method employing accurate numerical schemes for incompressible flow which applies to wings with oscillatory downwash conditions as well as to wings with steady-state downwash conditions.

The analysis of this paper is based on the linearized theory of compressible flow. The method used in making the calculations is somewhat similar to that used in reference 7 in that the calculation of the forces on a wing depends on the solution of an integral equation which relates the lift and downwash distributions. The unknown lift is expressed as a series of terms involving certain unknown coefficients. The method used herein differs from that in reference 7 chiefly in the manner of performing the surface integrations, which are obtained in a manner similar to that used in reference 8. For general application the surface integrals must be evaluated by numerical procedures; however, examination of the integrand for the special case of $M_o = 1.0$ shows that the chordwise integrations can be performed analytically, thus eliminating the need for any approximate or numerical procedure. In using this method for a value of M_o other than 1, the chordwise integration must be performed by numerical procedure. The final spanwise integration is performed by numerical procedures in either case.

The calculations are made for the wing alone and are compared with experimental data for the wing-body combination of reference 7. This method of comparison was used because calculations by the method of reference 7 for the wing alone and for the wing-body combination showed that the only effect of the presence of the body was to reduce the loading on the wing adjacent to the body. The loadings on the more important outboard sections were not appreciably affected.

SYMBOLS

$A = \left[1 - |\eta|(1 - \lambda)\right]$

AR aspect ratio, $\frac{4b^2}{S}$

A_n, a_{nm} coefficients in expression for lift (eqs. (2) and (4))

b wing semispan, ft

C_L	lift coefficient, $\frac{L}{qS}$
c	section chord, ft
c_o	$\frac{1}{2}$ root chord, ft
c_l	section lift coefficient
D	dimensionless spanwise interval between integration stations, referred to b (see sketch in section entitled "Spanwise Integration of Downwash")
F_n	spanwise integral over region n
$f(\eta)$	chordwise integral of lift (eq. (6))
g_r	complete chordwise integral at station r
K	kernel function
L	lift, $\int l \, dy$, lb
l	section lift, $\int \Delta l \, dx$, lb/ft
Δl	lift at any point, lb/sq ft
M_o	free-stream Mach number
q	dynamic pressure, $\frac{1}{2}\rho V^2$, lb/sq ft
S	wing area, sq ft
s	dimensionless semispan, $\frac{b}{c_o}$
V	airstream velocity, ft/sec
w	induced vertical velocity, ft/sec
x,ξ	dimensionless chordwise variable, referred to c_o
y,η	dimensionless spanwise variable, referred to b

α angle of attack, deg

$\beta = \sqrt{1 - M_o^2}$

δ unit length

ϵ dimensionless wing-chord distance from wing leading edge to control point (as function of η), referred to c_o

$\theta = \cos^{-1} \frac{2(\xi_m - \xi)}{\xi_{te} - \xi_{le}}$

Λ sweep angle for $\frac{1}{4}$-chord line, positive for sweepback, deg

λ taper ratio, $\frac{\text{Tip chord}}{\text{Root chord}}$

ν dimensionless chordwise variable, referred to c

ρ density of air, slugs/cu ft

Subscripts:

le leading edge

m midchord

te trailing edge

METHOD OF CALCULATION

The method used in making the calculations is similar to that used in reference 7 and is as follows:

Figure 1 shows a wing-panel diagram and the coordinate system used. The equation relating the lift distribution to the local induced velocity is given as

$$w(x,y) = -\frac{1}{4\pi\rho V} \iint_S \Delta l(\xi,\eta) K(x - \xi, y - \eta) d\xi \, d\eta \qquad (1)$$

where the kernel function for the case of subsonic flow is

$$K(x - \xi, y - \eta) = \frac{1}{b^2(y - \eta)^2}\left[1 + \frac{x - \xi}{\sqrt{(x - \xi)^2 + \beta^2(y - \eta)^2}}\right]$$

Note that for sonic flow ($\beta = 0$) the downwash at any control point is only affected by points ahead of the control point; that is, the increment in the bracket is 2 for $(x - \xi) > 0$ and becomes zero for $(x - \xi) < 0$. Thus, for $(x - \xi) \geqq 0$,

$$K(x - \xi, y - \eta) = \frac{2}{b^2(y - \eta)^2}$$

and for $(x - \xi) < 0$,

$$K(x - \xi, y - \eta) = 0$$

In this case it is noted that the kernel function depends only on the spanwise distance from the control point (x,y). The unknown lift distribution $\Delta l(\xi,\eta)$ in equation (1) is chosen to be expressed in the form of a series of loading terms in both spanwise and chordwise coordinates (ref. 7) as

$$\Delta l(\xi,\eta) = \frac{8\rho V^2 b}{c}\alpha\sqrt{1 - \eta^2}\left[\cot\frac{\theta}{2}\left(a_{00} + \eta a_{01} + \eta^2 a_{02} + \ldots\right) + \sin\theta\left(a_{10} + \eta a_{11} + \eta^2 a_{12} + \ldots\right) + \sin 2\theta\left(a_{20} + \eta a_{21} + \eta^2 a_{22} + \ldots\right) + \ldots\right]$$

In figure 1

$$\cos\theta = \frac{2(\xi_m - \xi)}{(\xi_{te} - \xi_{le})} = \frac{\left[|\eta| s \tan\Lambda - \left|\frac{\eta}{2}\right|(1 - \lambda) - \xi\right]}{\left[1 - |\eta|(1 - \lambda)\right]}$$

From this relation calculate $\cot\frac{\theta}{2}$, $\sin\theta$, and so forth, and substitute these in the expression for the lift distribution which becomes

$$\Delta l(\xi,\eta) = \frac{8\rho V^2 b}{c}\alpha\sqrt{1-\eta^2}\left(\sqrt{\frac{1+|\eta|s\tan\Lambda-\frac{3}{2}|\eta|(1-\lambda)-\xi}{1-|\eta|s\tan\Lambda-\frac{1}{2}|\eta|(1-\lambda)+\xi}}\left(a_{00}+\eta a_{01}+\eta^2 a_{02}+\cdots\right)+\right.$$

$$\frac{\sqrt{\left[1-|\eta|(1-\lambda)\right]^2-\left[|\eta|s\tan\Lambda-\frac{|\eta|}{2}(1-\lambda-\xi\right]^2}}{\left[1-|\eta|(1-\lambda)\right]}\left(a_{10}+\eta a_{11}+\eta^2 a_{12}+\cdots\right)+$$

$$\left\{\frac{|\eta|s\tan\Lambda-\frac{|\eta|}{2}(1-\lambda)-\xi}{2\left[1-|\eta|(1-\lambda)\right]^2}\right\}\sqrt{\left[1-|\eta|(1-\lambda)\right]^2-\left[|\eta|s\tan\Lambda-\frac{|\eta|}{2}(1-\lambda)-\xi\right]^2}$$

$$\left.\left(a_{20}+\eta a_{21}+\eta^2 a_{22}+\cdots\right)+\cdots\right) \qquad (2)$$

For sonic flow equation (1) now becomes

$$w(x,y) = -\frac{1}{2\pi\rho V}\int_{-1}^{1}\frac{d\eta}{s(y-\eta)^2}\int_{\xi_{le}}^{\xi_{te}\text{ or }x}\Delta l(\xi,\eta)d\xi \qquad (3)$$

where the double upper limit on the chordwise integral means that the integration stops at the trailing edge for values of η for which the trailing edge is forward of the control point but stops at x for values of η for which the trailing edge is rearward of the control point.

The problem now is to evaluate the integrals in equation (3) in order to determine the unknown coefficients a_{nm} appearing in the lift distribution $\Delta l(\xi,\eta)$. Since the local induced velocity $w(x,y)$ is assumed to be known, it may be seen that the integrations yield equations for $w(x,y)$ in terms of the unknown coefficients a_{nm} appearing in the lift distribution. Thus, by assuming the local induced velocity (local slope of mean camber line) to be known at a selected number of control points, a system of linear algebraic equations is obtained from which the coefficients a_{nm} can be determined. The selected number of control points, both spanwise and chordwise, correspond to the number of chordwise and spanwise terms retained in the equation.

Chordwise Integration of Downwash

In evaluating the integrals in equation (3), the procedure begins with the chordwise integration. However, the manner in which the spanwise integration is to be performed makes it desirable to divide each panel of the wing into an even number of sections of equal width with control points located on certain of the dividing lines. These section intervals must be small in order to secure accuracy in the spanwise integration. Then (for the $M_0 = 1.0$ case) for each control point, the chordwise integration is analytically performed along every dividing line as indicated in equation (3). It is seen that the chordwise integration in equation (3) involves only an integration of the lift distribution (eq. (2)), which becomes (for a wing having lateral symmetry)

$$\int_{\xi_{le}}^{\xi_{te} \text{ or } \xi_{le}+\epsilon} \Delta l(\xi,\eta)d\xi = EA_0\left[\sqrt{\epsilon(2A - \epsilon)} + 2A \tan^{-1}\sqrt{\frac{\epsilon}{2A - \epsilon}}\right] -$$

$$EA_1\left[\frac{A - \epsilon}{2A}\sqrt{\epsilon(2A - \epsilon)} - A \tan^{-1}\sqrt{\frac{\epsilon}{2A - \epsilon}}\right] +$$

$$EA_2\left\{\left(\frac{2}{3A^2}\right)\left[\epsilon(2A - \epsilon)\right]^{3/2}\right\} +$$

$$EA_3\left\{\left(\frac{A - \epsilon}{A^3}\right)\left[\epsilon(2A - \epsilon)\right]^{3/2}\right\} + \ldots \qquad (4)$$

where

$$E = \frac{4\rho V^2 s \tan\alpha}{A}\sqrt{1 - \eta^2}$$

$$A = \left[1 - \eta(1 - \lambda)\right] = \frac{\xi_{te} - \xi_{le}}{2}$$

and

$$A_0 = \left(a_{00} + \eta^2 a_{02} + \eta^4 a_{04} + \ldots + \eta^m a_{0m}\right)$$

$$A_1 = \left(a_{10} + \eta^2 a_{12} + \eta^4 a_{14} + \ldots + \eta^m a_{1m}\right)$$

. . . . . .

$$A_n = \left(a_{n0} + \eta^2 a_{n2} + \eta^4 a_{n4} + \ldots + \eta^m a_{nm}\right)$$

and where

$$\epsilon = \frac{\text{Wing chord distance from leading edge to control point}}{c_o}$$

Substituting the expression for the lift given in equation (4) into the integral equation (eq. (3)) gives the expression for the total local downwash:

$$w(x,y) = \frac{2V \tan \alpha}{\pi} \int_{-1}^{1} \frac{f(\eta)}{(y - \eta)^2} \, d\eta \qquad (5)$$

where $f(\eta)$ equals the chordwise integral of the lift along any particular chord and is given as

$$f(\eta) = \frac{\sqrt{1 - \eta^2}}{A}\left(A_0\left[\sqrt{\epsilon(2A - \epsilon)} + 2A \tan^{-1}\sqrt{\frac{\epsilon}{2A - \epsilon}}\right] - A_1\left[\frac{A - \epsilon}{2A}\sqrt{\epsilon(2A - \epsilon)} - A \tan^{-1}\sqrt{\frac{\epsilon}{2A - \epsilon}}\right] + A_2\left\{\frac{2}{3A^2}\sqrt{\left[\epsilon(2A - \epsilon)\right]^3}\right\} + A_3\left\{\frac{A - \epsilon}{A^3}\sqrt{\left[\epsilon(2A - \epsilon)\right]^3} + \ldots\right\}\right)$$

Spanwise Integration of Downwash

As mentioned in the preceding section, the wing is divided into a fairly large, even number of sections of equal width in order to secure accuracy in the spanwise integration as shown in the following sketch:

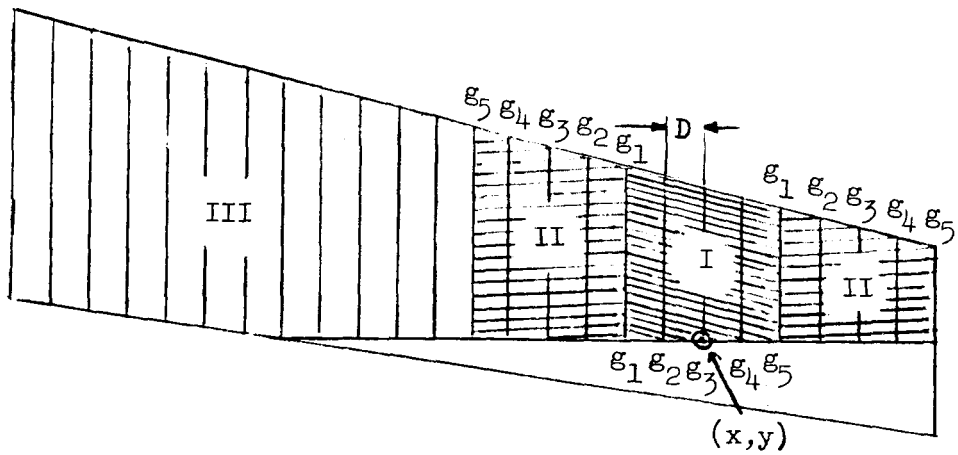

The sketch shows one panel of a wing, where the distance D represents the spanwise interval in the spanwise numerical integration. The sketch shows that the chordwise integrations extend from the leading edge to x or to the trailing edge, as has been previously noted.

After evaluating the chordwise integrals along every dividing line, the spanwise integration across the entire wing was performed by numerical methods. In order to expedite this integration and retain a high degree of accuracy and in order to handle the singularity at $\eta = y$, the integration is performed as a sum of three different integrals, by fixing the proper limits of integration of each region of the wing.

Thus, the integral in equation (5) may be written

$$\int_{-1}^{1} \frac{f(\eta)}{(y - \eta)^2}\, d\eta = F_I + F_{II} + F_{III} \qquad (6)$$

where the integrals F_I, F_{II}, and F_{III} correspond to the regions I, II, and III shown in the sketch.

In order to obtain the integral F_{III} for region III, the calculated chordwise integrals $f(\eta)$ were divided by the appropriate value of $(y - \eta)^2$ and the spanwise integration was performed by Simpson's rule. For region III to the left of the control point, for example,

$$F_{III} = \int_{-s}^{y-nD} \frac{f(\eta)}{(y-\eta)^2}\,d\eta = \sum \frac{D}{3}\left[\frac{g_1}{(y-\eta_1)^2} + \frac{4g_2}{(y-\eta_2)^2} + \frac{2g_3}{(y-\eta_3)^2} + \frac{4g_4}{(y-\eta_4)^2} + \cdots\right] \tag{7}$$

where n, in the upper limit, is the number of divisions from the control point to the first point considered in region III.

In region I, across the control point (x,y), and region II, adjacent to the control point, other analytical methods were necessary. In the integral F_{II} for region II the integrals change too rapidly for safe use of Simpson's rule; the integral F_I for region I involves the singularity at $\eta = y$. A complete treatment of the singularity in the integral (in region I) is given by Mangler in appendix I of reference 6. For regions I and II special rules were developed which analytically took into account the term $(y - \eta)^2$. Lagrangian interpolation methods were used to develop an analytic function for $f(\eta)$ in terms of the calculated chordwise integrals. The integral of this function divided by $(y - \eta)^2$ was then obtained.

As an example, when $f(\eta)$ in region I (across the control point) was represented by a parabola, the following three-point integration rule was obtained:

$$F_I = \int_{y-D}^{y+D} \frac{f(\eta)}{(y-\eta)^2}\,d\eta = \frac{1}{D}\left(g_1 - 4g_2 + g_3\right) \tag{8a}$$

where

$$D = \frac{\text{Interval between lines or vortex width}}{b}$$

For a five-point (see sketch) integration across the control point (x,y), that is, from $(y + 2D)$ to $(y - 2D)$, the following integral relation is obtained:

$$F_I = \int_{y-2D}^{y+2D} \frac{f(\eta)}{(y-\eta)^2}\,d\eta = \frac{1}{18D}\left(g_1 + 32g_2 - 84g_3 + 32g_4 + g_5\right) \tag{8b}$$

For region II adjacent to the control point (x,y), the integration for a three-point solution is given by

$$F_{II} = \int_{\delta}^{\delta+2D} \frac{f(\eta)}{(y-\eta)^2}\,d\eta = \frac{1}{D\delta(\delta+2D)}\left[\left(2\delta^2 + 5\delta D + 2D^2\right)g_1 - 4\delta(\delta+2D)g_2 + \left(2\delta^2 + 3\delta D\right)g_3\right] - \frac{1}{2D^2}\log_e\frac{\delta+2D}{\delta}\left[(2\delta+3D)g_1 - 4(\delta+D)g_2 + (2\delta+D)g_3\right] \tag{9a}$$

where $\delta = D$ times the number of spaces to the limit of region I. For the case of a five-point integration across the control point (x,y), as shown in the sketch, $\delta = 2D$.

For region II, the integration of a five-point solution (see sketch) is given by

$$F_{II} = \int_{\delta}^{\delta+4D} \frac{f(\eta)}{(y+\eta)^2}\,d\eta = \frac{1}{9D^3\delta(\delta+4D)}\left[g_1\left(6\delta^4 + 57\delta^3 D + 179\delta^2 D^2 + 197\delta D^3 + 36D^4\right) - g_2\left(24\delta^4 + 210\delta^3 D + 572\delta^2 D^2 + 464\delta D^3\right) + g_3\left(36\delta^4 + 288\delta^3 D + 678\delta^2 D^2 + 408\delta D^3\right) - g_4\left(24\delta^4 + 174\delta^3 D + 356\delta^2 D^2 + 176\delta D^3\right) + g_5\left(6\delta^4 + 39\delta^3 D + 71\delta^2 D^2 + 35\delta D^3\right)\right] - \frac{1}{24D^4}\log_e\frac{\delta+4D}{\delta}\left[g_1\left(4\delta^3 + 30\delta^2 D + 70\delta D^2 + 50D^3\right) - g_2\left(16\delta^3 + 108\delta^2 D + 208\delta D^2 + 96D^3\right) + g_3\left(24\delta^3 + 144\delta^2 D + 228\delta D^2 + 72D^3\right) - g_4\left(16\delta^3 + 84\delta^2 D + 112\delta D^2 + 32D^3\right) + g_5\left(4\delta^3 + 18\delta^2 D + 22\delta D^2 + 6D^3\right)\right] \tag{9b}$$

The spanwise integral of equation (5) to obtain the value of $w(x,y)$ is now given by the sum of the three integral parts; that is,

$$w(x,y) = \frac{2V \tan \alpha}{\pi} \int_{-1}^{1} \frac{f(\eta)}{(y - \eta)^2} d\eta = \frac{2V \tan \alpha}{\pi A}\left(F_I + F_{II} + F_{III}\right) \qquad (10)$$

The results obtained in equation (10) express the downwash, at the control point (x,y) in terms of the ordinates of $f(\eta)$ by the sum of the results in equations (7) to (9). This sum in turn expresses the downwash as a linear expression in the unknown coefficients a_{nm}. (See eq. (5).) By evaluating the integrals for $n \times m$ control points, where the local slope of the mean camber line at each control point is known, a system of algebraic equations is obtained from which the coefficients a_{nm} can be determined.

L 3 4 4

Calculation of Aerodynamic Characteristics

The element lift for any point on the wing is given in equation (2) by

$$\Delta l(\xi,\eta) = \frac{8\rho V^2 b \tan \alpha}{c}\sqrt{1 - \eta^2}\left\{\sqrt{\frac{1 + |\eta| s \tan \Lambda - \frac{3}{2}|\eta|(1 - \lambda) - \xi}{1 - |\eta| s \tan \Lambda - \frac{1}{2}|\eta|(1 - \lambda) + \xi}}\left(a_{00} + \eta a_{01} + \eta^2 a_{02} + \cdots\right) + \right.$$

$$\frac{\sqrt{A^2 - \left[|\eta| s \tan \Lambda - \frac{|\eta|}{2}(1 - \lambda) - \xi\right]^2}}{A}\left(a_{10} + \eta a_{11} + \eta^2 a_{12} + \cdots\right) +$$

$$\left.\frac{|\eta| s \tan \Lambda - \frac{|\eta|}{2}(1 - \lambda) - \xi}{2A^2}\sqrt{A^2 - \left[|\eta| s \tan \Lambda - \frac{|\eta|}{2}(1 - \lambda) - \xi\right]^2}\left(a_{20} + \eta a_{21} + \eta^2 a_{22} + \cdots\right) + \cdots\right\}$$

or the total lift (per unit span) on any chord is (note that $c = 2c_0 A$)

$$l = \frac{4\rho V^2 s c_0}{A} \tan \alpha \sqrt{1 - \eta^2} \int_{-\xi_{le}}^{\xi_{te}} \Delta l(\xi,\eta) d\xi$$

$$= \frac{4\rho V^2 c_0 s}{A} \tan \alpha \sqrt{1 - \eta^2}\left(l_1 + l_2 + l_3 + \cdots\right) \qquad (11)$$

where

$$l_1 = \left(a_{00} + \eta a_{01} + \eta^2 a_{02} + \ldots\right) \int_{-\left[1-s|\eta|\tan\Lambda - \frac{|\eta|}{2}(1-\lambda)\right]}^{\left[1+s|\eta|\tan\Lambda - \frac{3}{2}|\eta|(1-\lambda)\right]} \sqrt{\frac{1 + s|\eta| \tan\Lambda - \frac{3}{2}|\eta|(1-\lambda) - \xi}{1 - s|\eta| \tan\Lambda - \frac{1}{2}|\eta|(1-\lambda) + \xi}}\, d\xi$$

and so forth. On chordwise integration

$$l_1 = \left(a_{00} + \eta a_{01} + \eta^2 a_{02} + \ldots\right)\pi A$$

$$l_2 = \left(a_{10} + \eta a_{11} + \eta^2 a_{12} + \ldots\right)\frac{\pi}{2} A$$

$$l_3,\ l_4,\ \ldots\ l_\eta = 0$$

For a symmetrical wing for three spanwise control-point locations, the total lift (per unit span) on any chord is given by

$$l = \frac{4\rho V^2 c_o s}{A} \tan\alpha\sqrt{1 - \eta^2}A\pi\left[\left(a_{00} + \eta^2 a_{02} + \eta^4 a_{04}\right) + \frac{1}{2}\left(a_{10} + \eta^2 a_{12} + \eta^4 a_{14}\right)\right] \tag{12}$$

or the section lift coefficient is

$$c_l = \frac{8\pi c_o s}{c} \tan\alpha\sqrt{1 - \eta^2}\left[\left(a_{00} + \eta^2 a_{02} + \eta^4 a_{04}\right) + \frac{1}{2}\left(a_{10} + \eta^2 a_{12} + \eta^4 a_{14}\right)\right] \tag{13}$$

But the total lift on the wing is

$$L = \int_{-s}^{s} l\, dy$$

or

$$C_L = \frac{\int_{-1}^{1} l\, d\eta}{\frac{1}{2}\rho V^2 S} \tag{14}$$

$$C_L = \frac{4\pi\rho V^2 b^2 \tan\alpha}{\frac{1}{2}\rho V^2 S} \int_{-1}^{1} \sqrt{1 - \eta^2}\left[\left(a_{00} + \eta^2 a_{02} + \eta^4 a_{04}\right) + \frac{1}{2}\left(a_{10} + \eta^2 a_{12} + \eta^4 a_{14}\right)\right] d\eta \tag{15}$$

$$C_L = \frac{8\pi b^2 \tan\alpha}{S}\left[\frac{\pi}{2}\left(a_{00} + \frac{1}{2}a_{10}\right) + \frac{\pi}{8}\left(a_{02} + \frac{1}{2}a_{12}\right) + \frac{\pi}{16}\left(a_{04} + \frac{1}{2}a_{14}\right)\right] \tag{16}$$

For

$$AR = \frac{4b^2}{S}$$

the lift coefficient becomes

$$C_L = \frac{\pi^2 AR \tan\alpha}{16}\left(16a_{00} + 8a_{10} + 4a_{02} + 2a_{12} + 2a_{04} + a_{14}\right) \tag{17}$$

The slope of the lift curve is

$$\frac{dC_L}{d\alpha} = \frac{\pi^2 AR}{16}\left(16a_{00} + 8a_{10} + 4a_{02} + 2a_{12} + 2a_{04} + a_{14}\right) \tag{18}$$

The ratio of the section lift coefficient c_l at any station y to the total lift coefficient C_L is

$$\frac{c_l}{C_L} = \frac{32S\sqrt{1 - \eta^2}}{\pi bc} \frac{\left(a_{00} + \frac{1}{2}a_{10}\right) + \eta^2\left(a_{02} + \frac{1}{2}a_{12}\right) + \eta^4\left(a_{04} + \frac{1}{2}a_{14}\right)}{\left(16a_{00} + 8a_{10} + 4a_{02} + 2a_{12} + 2a_{04} + a_{14}\right)} \tag{19}$$

MODEL AND PROCEDURE

The wing plan form and details of the wing-body configuration are shown in figure 2. The wing $\frac{1}{4}$-chord line was swept back 45°; the wing had an aspect ratio of 4 and a taper ratio of 0.15. The wing airfoil section at the midspan was NACA 64A206, a = 0 which faired into an NACA 64A203, a = 0.8 (modified) airfoil section at the 0.5-semispan location and retained this section from the midspan to the wing tip. Calculations were made for the wing alone. The experimental data used in the comparisons were obtained from tests made in the Langley 8-foot transonic tunnel on the same wing in combination with the body. (Details of the body are given in fig. 2.) Other experimental data and further details of the wing-body combination are given in reference 9.

Mean camber lines, in percent chord, of two wing sections are shown in figure 3. The sections shown correspond to the spanwise control-point locations. Besides the camber built into the sections, there is a wing twist due to aeroelastic effects when the wing experiences lift. Influence coefficients due to normal-force and pitching-moment loads were obtained by static-deflection calibrations of the wing in order to evaluate the wing twist due to aeroelastic effects. The spanwise variation of twist for the wing-body configurations for an angle of attack of 4.0° is shown in figure 4 for $M_0 = 0.98$ and $M_0 = 1.03$. The calculated loadings were made on the assumption that the wing at $M_0 = 1.0$ was pretwisted by an average value of the curves for $M_0 = 0.98$ and $M_0 = 1.03$.

Twelve control-point locations were chosen for the calculations made by the method presented herein. Calculations were made for all 12 points and for several combinations of 9 control points. The exact locations of the control points, both chordwise and spanwise, are given in table I. The spanwise locations were chosen at 0.25, 0.50, and 0.80 of the semispan. The chordwise locations in each case were selected so that if the Mach line through the control point intersected the leading edge, the intersection occurred at the same spanwise location as the division made for integration purposes. These selections, chosen so that no fractional spanwise divisions resulted, were made purely to simplify the spanwise integration.

COMPARISON OF EXPERIMENTAL AND CALCULATED RESULTS

Figure 5 shows a comparison of the calculated and the experimentally measured spanwise loading plotted against the wing semispan. The

calculated data are tabulated in table II. The data are for an angle of attack of 4.0°. The experimental data are for the wing-body combination shown in figure 2, since no experimental data were obtained for the wing alone. Also these data are presented for Mach numbers of 0.98 and 1.03 since no experimental data were obtained for $M_0 = 1.0$. All of the calculated data are for the wing alone and for a Mach number of 1.0. The comparison of computed data for the wing alone with the experimental data for the wing-body configuration is made on the basis of the good agreement between calculated data for the wing alone and those for the wing-body configuration at subsonic speeds shown in reference 7, where only an empirical method for correcting for the body was presented. The shape or distribution of the loading for the calculated data at $M_0 = 1.0$ is about the same as the shape of the experimental curves for $M_0 = 0.98$ and $M_0 = 1.03$. The magnitude of the lift for the calculated data for $M_0 = 1.0$ is about 10 percent higher than the experimental data at $M_0 = 0.98$ which is greater than the value for $M_0 = 1.03$. Of particular interest, however, is the agreement of the calculated spanwise distribution of lift, both in shape and magnitude, for the various selections of control points.

L
3
4
4

For the calculations using all 12 control points, or any combination of 9 points that was selected, the total calculated lift and the slope of the lift curve were essentially the same, the maximum variation from the mean value being ±1 percent. (See fig. 5.) Small variations in the distribution of the loading were found for each set of control points, the greatest variation for any 9 points being found for the 9 most forward control points. In these calculations only the effect of a change in the chordwise location of the control points was investigated; no changes were made in the locations of the control points in the spanwise direction. However, an examination of the method of spanwise integration shows that it is desirable to exclude control points from regions near the wing root or wing tip to insure accuracy in the spanwise integration. The data in figure 5 indicate that, for the method of integration used herein, for a wing of similar plan form and camber, the location of the control points is not a critical parameter in the calculation of the total wing loading or the span load distribution for the $M_0 = 1$ case. It appears that 9 control points located similarly to those in any of the sets used, may be sufficient since any set of 9 points, or all 12 points, give results in substantial agreement with the experimental data.

On the other hand, the method of reference 7 may not be applicable to a wing plan form of the shape used herein. For such a plan form the area ahead of the trailing-edge apex, which constitutes about two-thirds of the total wing area, cannot be affected by the region of the trailing edge, so that any analysis based essentially on two-dimensional subsonic-airfoil concepts would hardly be legitimate. The method, however, may

be applicable for a sweptback wing with a very high aspect ratio where a relatively smaller portion of the area ahead of the trailing-edge apex would be affected.

By way of illustration, spanwise loadings for the wing alone were calculated for $M_o = 1.0$ by the method of reference 7 and have been plotted against the wing semispan in figure 6 in order to obtain a comparison of results calculated by the two methods of integration. (Compare figs. 5 and 6.) (The wing twist under load shown in fig. 3 was also used in this case.) Also shown in figure 6 are the experimental data points (obtained for a wing-body combination) for $M_o = 0.98$ shown in figure 5. In order to obtain greater accuracy, the calculations in figure 6 were made for the 328-vortex pattern with eight load lines described in reference 10 instead of the 84-vortex pattern with four load lines used in reference 7. There are seven possible chordwise positions for the 328-vortex pattern but, when only three positions are used for the incompressible flow case, Falkner (ref. 10) recommended the 1/4, 1/2, and 3/4 chordwise locations. Similarly, when only three spanwise positions are used, the 0.2, 0.5, and 0.8 semispan stations were recommended. Table III gives the location of the control points used for the various solutions. The results of the calculations plotted in figure 6 are tabulated in table IV. Figure 6 and table IV show that the lift distributions obtained by this method of integration for the $M_o = 1.0$ case are critically dependent on the selection of control points. For example, solution 8 (control points at 1/4, 1/2, and 3/4 chordwise locations) or solution 9 (control points at 1/4, 1/2, and 7/8 chordwise locations) are both similar in shape to the experimental data. However, when all 12 of these points are used, solution 7, the shape is no longer in agreement, although it might be expected with more points that the agreement would be superior. In solution 10 (control points at 1/2, 3/4, and 7/8 chordwise locations), the discrepancy between calculated and experimental data becomes much greater, although it might have been expected that greater accuracy would be obtained with the control points towards the rear of the wing.

Figure 7 shows a comparison of data calculated by the method of reference 7 and the present method at a high subsonic speed, $M_o = 0.98$, for an angle of attack of 4.0°. The experimental data for $M_o = 0.98$ are also shown in the figure. The data calculated by the method of reference 7 are for the wing-body combination of the experimental data taken from reference 9, but the data for the method used herein are for the wing alone. In the latter case it was necessary to perform the chordwise integration by numerical procedures. The same wing twist under load (see fig. 3) and the same control-point locations were used for both sets of calculations. The calculations were made for two sets of control

points by the method in this report and, as was found at $M_o = 1.0$, there was a small difference in the total lift and in the distribution of lift for a change in control-point location (fig. 7).

CONCLUDING REMARKS

A detailed method for calculating the aerodynamic loading on a thin wing at a Mach number of 1.0 is presented. A comparison of the calculated load distributions with experimental results indicated that, for the wing tested, the magnitude and distribution of the calculated spanwise loading are in good agreement with experiment at a Mach number of 1.0.

Langley Research Center,
National Aeronautics and Space Administration,
Langley Field, Va., May 27, 1959.

REFERENCES

1. Mangler, K. W.: Calculation of the Pressure Distribution Over a Wing at Sonic Speeds. R. & M. No. 2888, British A.R.C., Sept. 1951.

2. Heaslet, Max. A., Lomax, Harvard, and Spreiter, John R.: Linearized Compressible-Flow Theory for Sonic Flight Speeds. NACA Rep. 956, 1950. (Supersedes NACA TN 1824.)

3. Klunker, E. B., and Harder, Keith C.: General Solutions for Flow Past Slender Cambered Wings With Swept Trailing Edges and Calculation of Additional Loading Due to Control Surfaces. NACA TN 4242, 1958.

4. Heaslet, Max. A., and Spreiter, John R.: Three-Dimensional Transonic Flow Theory Applied to Slender Wings and Bodies. NACA Rep. 1318, 1957. (Supersedes NACA TN 3717.)

5. Falkner, V. M.: The Calculation of Aerodynamic Loading on Surfaces of any Shape. R. & M. No. 1910, British A.R.C., Aug. 1943.

6. Multhopp, H.: Methods for Calculating the Lift Distribution of Wings (Subsonic Lifting Surface Theory). Rep. No. Aero. 2353, British R.A.E., Jan. 1950.

7. Crigler, John L.: Comparison of Calculated and Experimental Load Distributions on Thin Wings at High Subsonic and Sonic Speeds. NACA TN 3941, 1957.

8. Watkins, Charles E., Woolston, Donald S., and Cunningham, Herbert J.: A Systematic Kernel Function Procedure for Determining Aerodynamic Forces on Oscillating or Steady Finite Wings at Subsonic Speeds. NASA TR R-48, 1959.

9. Fischetti, Thomas L.: Investigation at Mach Numbers From 0.80 to 1.43 of Pressure and Load Distributions Over a Thin 45° Sweptback Highly Tapered Wing in Combination With Basic and Indented Bodies. NACA RM L57D29a, 1957.

10. Falkner, V. M.: The Solution of Lifting-Plane Problems by Vortex-Lattice Theory. R. & M. No. 2591, British A.R.C., 1953.

TABLE I

CHORDWISE AND SPANWISE LOCATION OF CONTROL POINTS

	Location of control point -											
	1	2	3	4	5	6	7	8	9	10	11	12
η	0.25	0.50	0.80	0.25	0.50	0.80	0.25	0.50	0.80	0.25	0.50	0.80
ν	0.173	0.237	0.213	0.519	0.474	0.426	0.778	0.711	0.852	0.952	0.948	0.938

TABLE II

CALCULATED LIFT COEFFICIENTS FOR $M_o = 1.0$ AND $\alpha = 4.0^o$

Section lift coefficients for -						
$\eta = 0.12$	$\eta = 0.25$	$\eta = 0.40$	$\eta = 0.60$	$\eta = 0.80$	$\eta = 0.90$	$\eta = 0.95$
Solution 1; 12 control points; $\frac{dC_L}{d\alpha} = 0.1065$						
0.512	0.511	0.502	0.463	0.340	0.240	0.170
Solution 2; control points 1, 2, 3, 4, 5, 6, 7, 8, 9; $\frac{dC_L}{d\alpha} = 1.067$						
0.555	0.538	0.500	0.430	0.318	0.235	0.172
Solution 3; control points 1, 2, 3, 4, 5, 6, 10, 11, 12; $\frac{dC_L}{d\alpha} = 0.1085$						
0.532	0.530	0.518	0.465	0.341	0.235	0.165
Solution 4; control points 1, 2, 3, 7, 8, 9, 10, 11, 12; $\frac{dC_L}{d\alpha} = 0.1078$						
0.517	0.516	0.505	0.461	0.347	0.246	0.170
Solution 5; control points 4, 5, 6, 7, 8, 9, 10, 11, 12; $\frac{dC_L}{d\alpha} = 0.1073$						
0.530	0.526	0.509	0.452	0.334	0.240	0.162
Solution 6; control points 4, 5, 6, 7, 8, 9; $\frac{dC_L}{d\alpha} = 0.1065$						
0.555	0.532	0.495	0.420	0.315	0.232	0.170

TABLE III

LOCATION OF CONTROL POINTS FOR CALCULATIONS

BY METHOD OF REFERENCE 7

	Location of control point -											
	1	2	3	4	5	6	7	8	9	10	11	12
η	0.20	0.50	0.80	0.20	0.50	0.80	0.20	0.50	0.80	0.20	0.50	0.80
ν	$\frac{1}{4}$	$\frac{1}{4}$	$\frac{1}{4}$	$\frac{1}{2}$	$\frac{1}{2}$	$\frac{1}{2}$	$\frac{3}{4}$	$\frac{3}{4}$	$\frac{3}{4}$	$\frac{7}{8}$	$\frac{7}{8}$	$\frac{7}{8}$

TABLE IV

LIFT COEFFICIENTS CALCULATED BY METHOD OF REFERENCE 1

FOR $M_o = 1.0$ AND $\alpha = 4.0^o$

Section lift coefficients for -					
$\eta = 0.25$	$\eta = 0.40$	$\eta = 0.60$	$\eta = 0.80$	$\eta = 0.90$	$\eta = 0.95$
Solution 7; 12 control points (see table III); $\frac{dC_L}{d\alpha} = 0.118$					
0.400	0.452	0.515	0.540	0.460	0.357
Solution 8; control points 1, 2, 3, 4, 5, 6, 7, 8, 9; $\frac{dC_L}{d\alpha} = 0.1190$					
0.575	0.556	0.501	0.382	0.271	0.192
Solution 9; control points 1, 2, 3, 4, 5, 6, 10, 11, 12; $\frac{dC_L}{d\alpha} = 0.1103$					
0.538	0.518	0.455	0.341	0.243	0.172
Solution 10; control points 1, 2, 3, 7, 8, 9, 10, 11, 12; $\frac{dC_L}{d\alpha} = 0.0679$					
-0.095	0.142	0.516	0.715	0.644	0.501
Solution 11; control points 4, 5, 6, 7, 8, 9; $\frac{dC_L}{d\alpha} = 0.0996$					
0.534	0.465	0.360	0.258	0.197	0.149

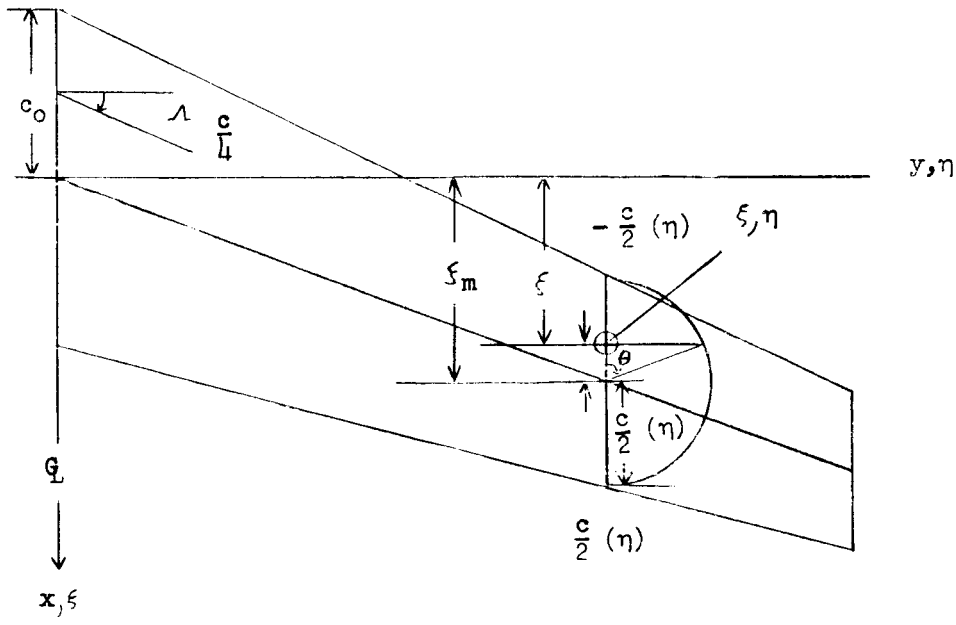

$$\xi_{le} = -\left[1 - s\,\eta \tan\Lambda - \frac{\eta}{2}(1-\lambda)\right]$$

$$\xi_{te} = \left[1 + s\,\eta \tan\Lambda - 3\,\frac{\eta}{2}(1-\lambda)\right]$$

$$\xi_{te} - \xi_{le} = 2\left[1 - \eta(1-\lambda)\right]$$

$$\xi_m = \eta\left[s \tan\Lambda - \frac{1}{2}(1-\lambda)\right]$$

$$\cos\theta = \frac{2(\xi_m - \xi)}{\xi_{te} - \xi_{le}} = \frac{\left[\eta\, s \tan\Lambda - \frac{\eta}{2}(1-\lambda) - \xi\right]}{\left[1 - \eta(1-\lambda)\right]}$$

Figure 1.- Wing-panel diagram and coordinate system.

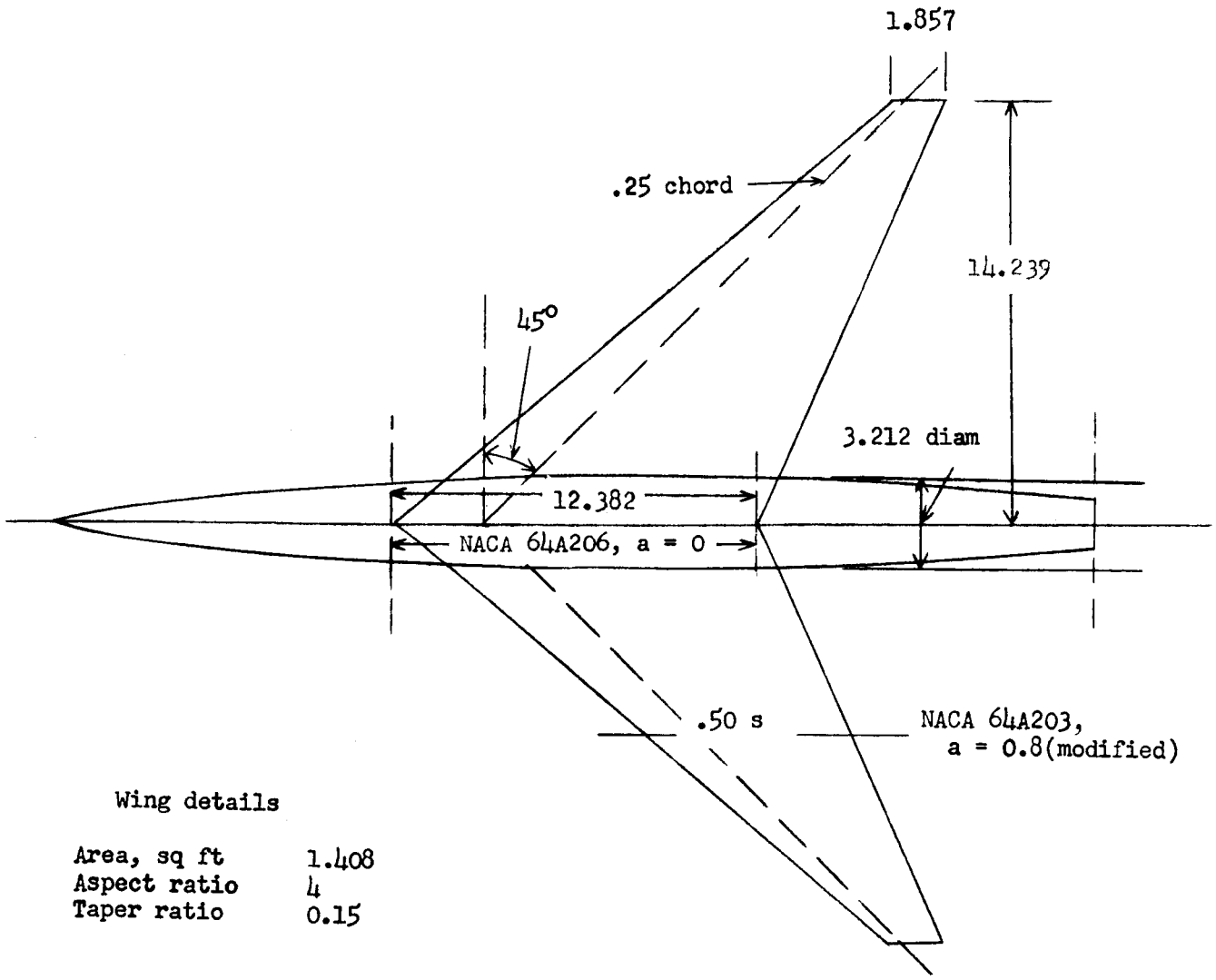

Figure 2.- Details of wing-body configuration. All dimensions are in inches.

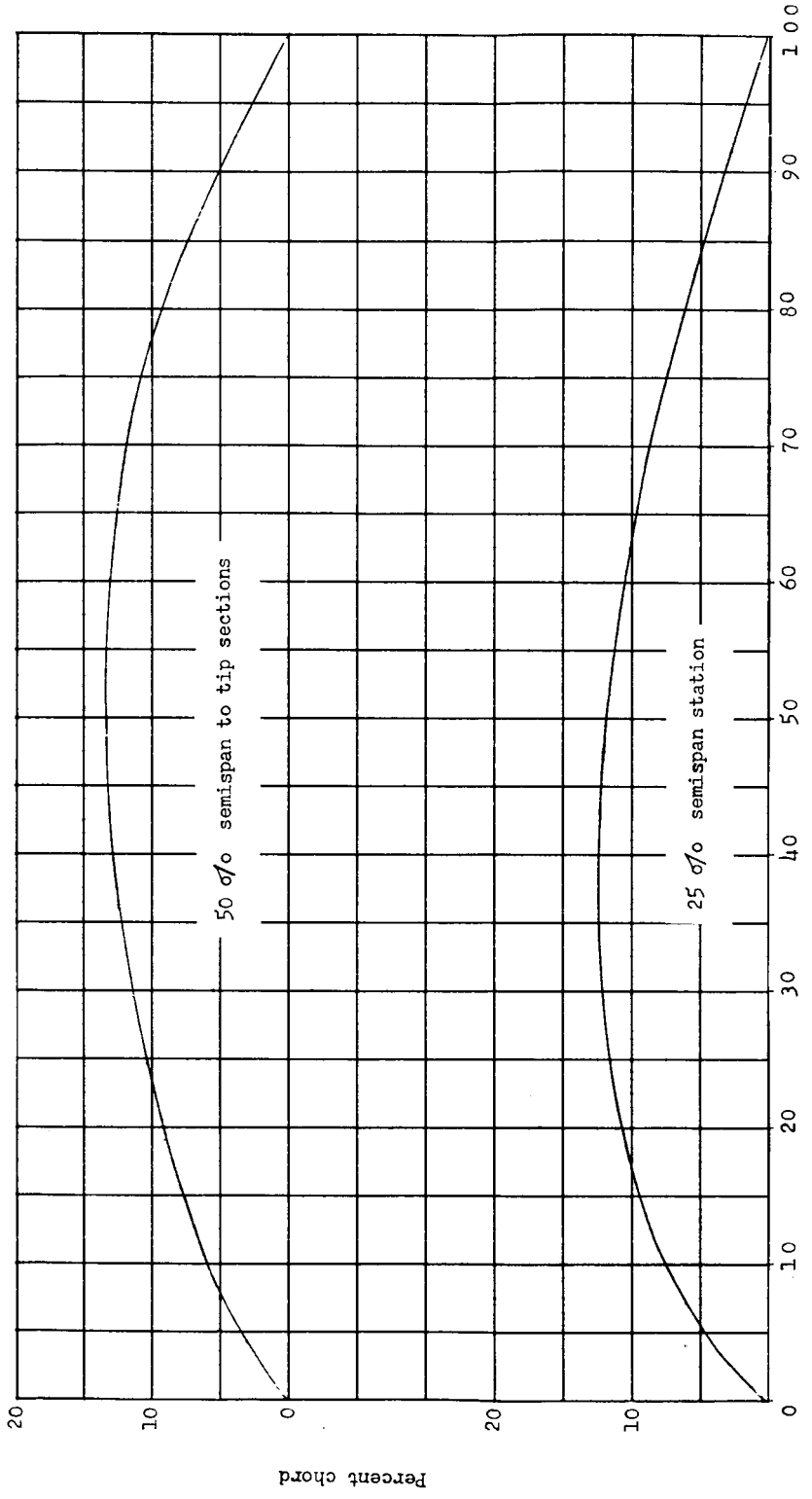

Figure 3.- Mean camber lines of wing sections.

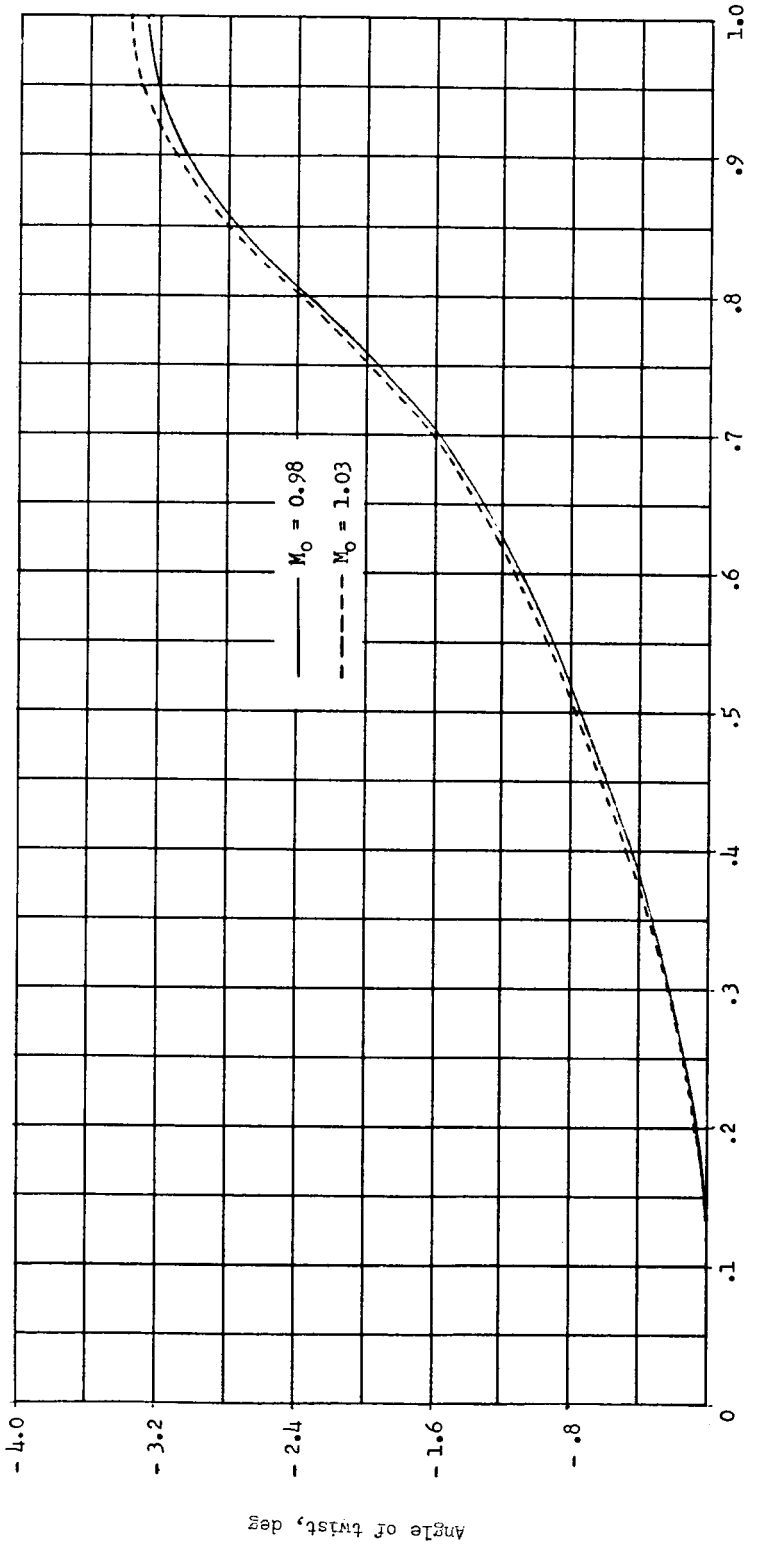

Figure 4.- Calculated variation of wing twist due to aeroelasticity. $\alpha = 4.0^{\circ}$.

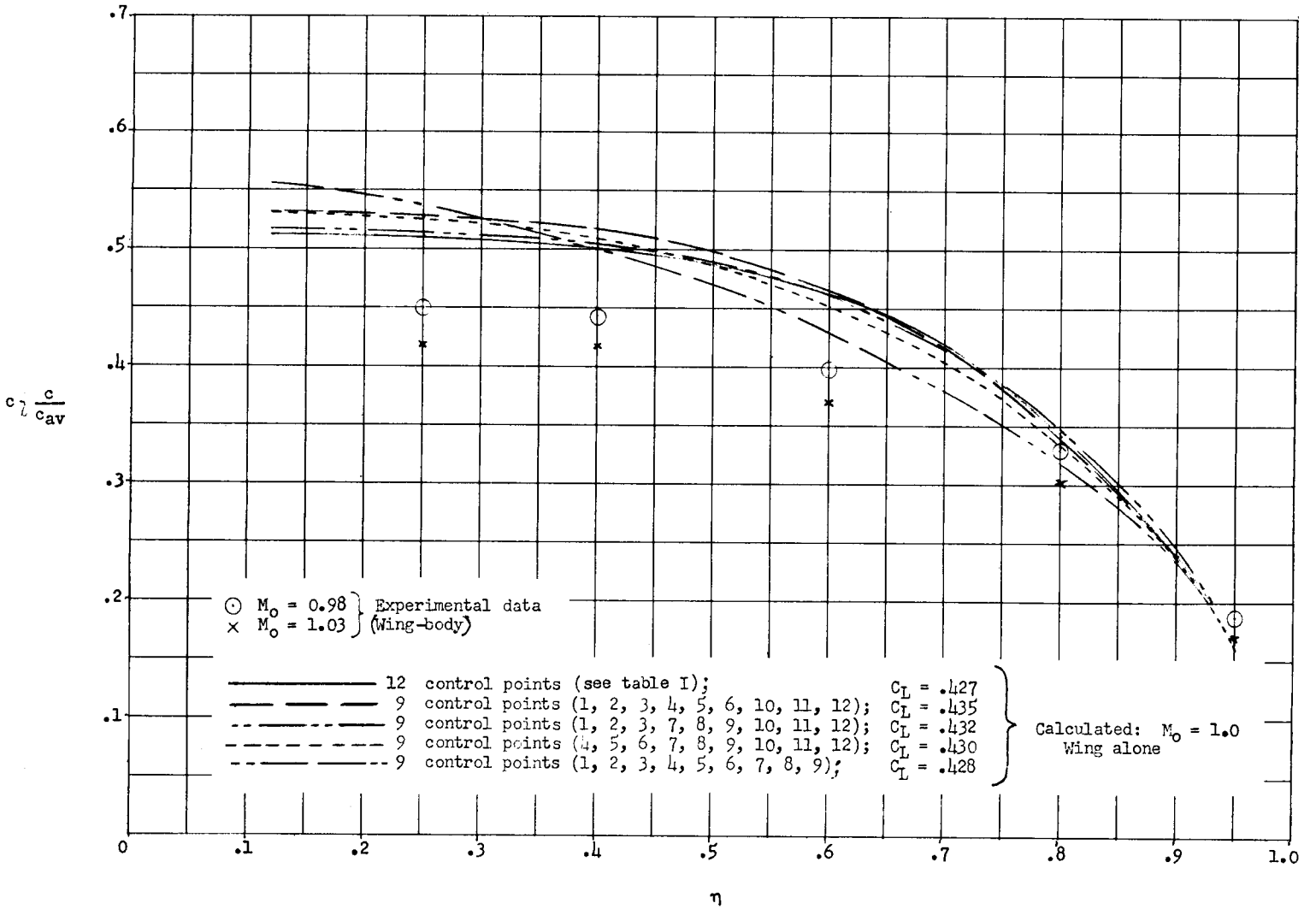

Figure 5.- Comparison of calculated and experimental spanwise loadings. $\alpha = 4.0^\circ$.

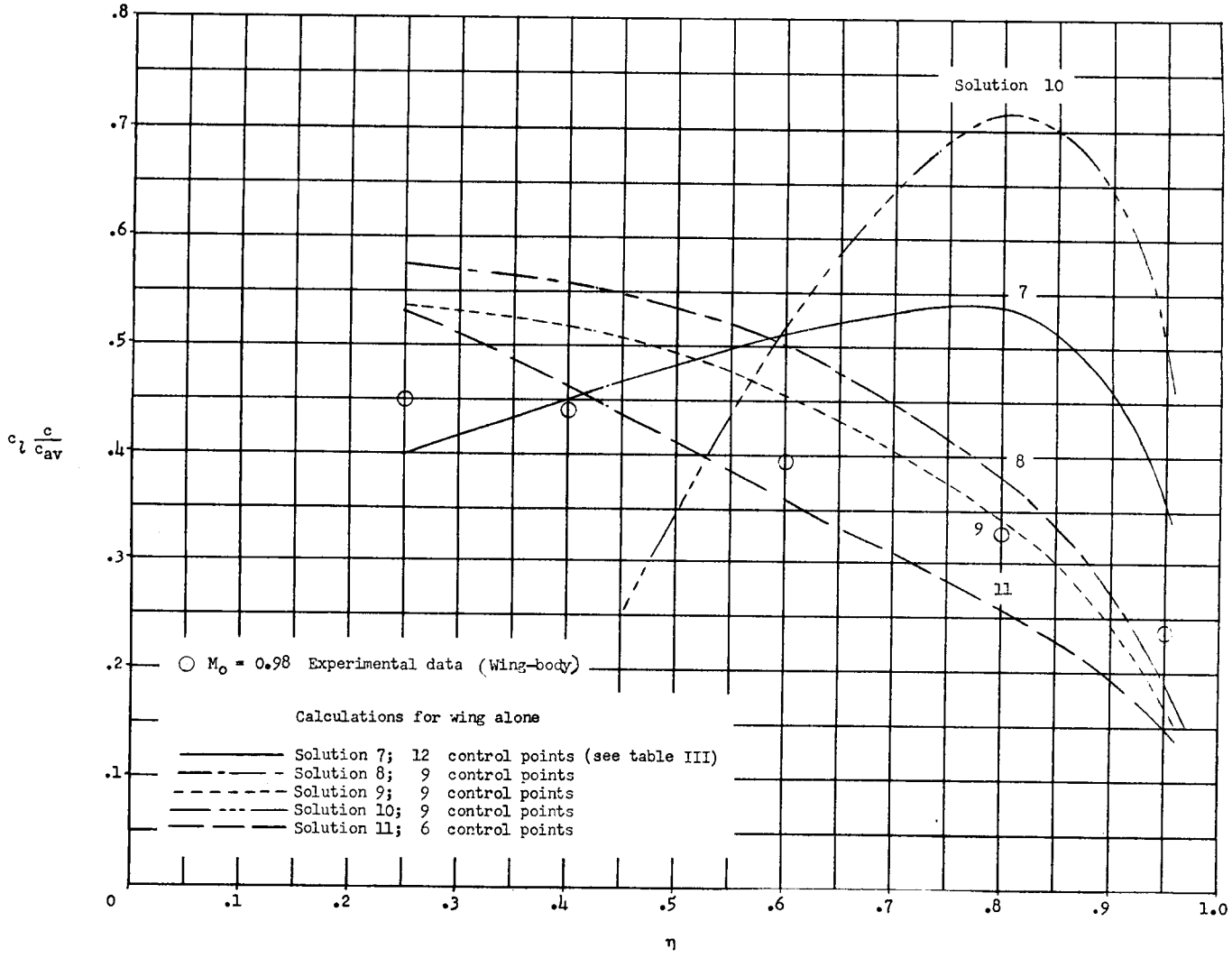

Figure 6.- Effect of control-point locations on calculated spanwise loadings (calculated by method of ref. 7). $\alpha = 4.0^{\circ}$; $M_o = 1.0$.

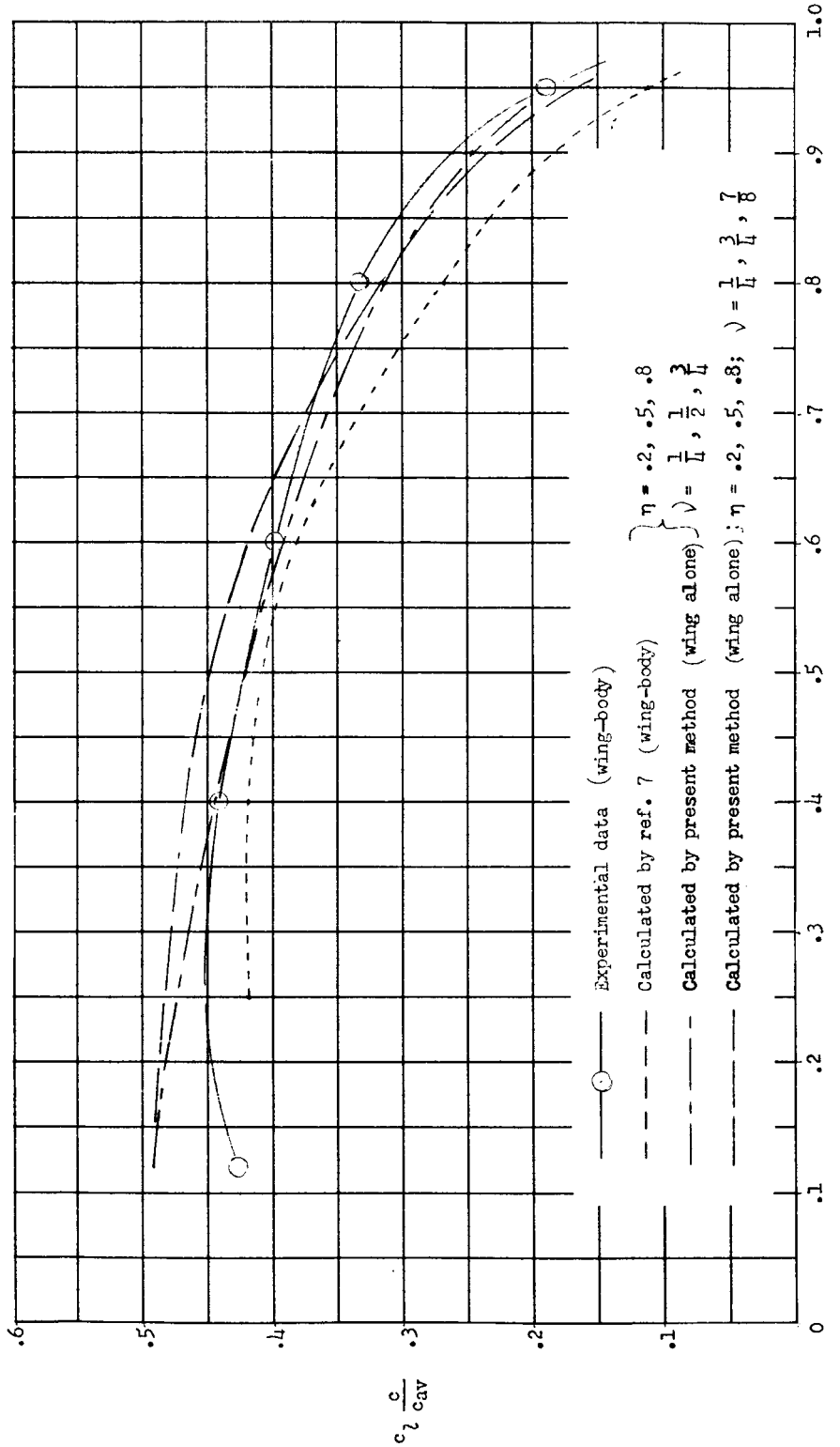

Figure 7.- Comparison of calculated and experimental spanwise loadings. $\alpha = 4.0^{\circ}$; $M_o = 0.98$.